

Geophysical Research Letters[®]



RESEARCH LETTER

10.1029/2023GL104991

Carsten Abraham and Colin Goldblatt
contributed equally to this work

Systematic Occurrence Cycle of Typical RH-Profiles During the MJO: Evidence for Ubiquitous Pre-Moistening

Carsten Abraham^{1,2} , Colin Goldblatt² , and Adrian J. Matthews³ 

¹Canadian Centre for Climate Modelling and Analysis, Environment and Climate Change Canada, Victoria, BC, Canada,

²School of Earth and Ocean Sciences, University of Victoria, Victoria, BC, Canada, ³Centre for Ocean and Atmospheric Sciences, School of Environmental Sciences and School of Mathematics, University of East Anglia, Norwich, UK

Key Points:

- The occurrence probabilities (OP) of characteristic tropical RH-profile classes change systematically with each phase of the MJO-cycle
- About 10 days prior deep convection cores RH-profiles shift from constantly dry to linearly decreasing, a mid-tropospheric pre-moistening
- Analyzing OPs of RH-classes during the Madden–Julian Oscillation can serve as a process-based diagnostic to identify misrepresented processes in climate models

Correspondence to:

C. Abraham,
carsten.abraham@ec.gc.ca

Citation:

Abraham, C., Goldblatt, C., & Matthews, A. J. (2023). Systematic occurrence cycle of typical RH-profiles during the MJO: Evidence for ubiquitous pre-moistening. *Geophysical Research Letters*, 50, e2023GL104991. <https://doi.org/10.1029/2023GL104991>

Received 15 JUN 2023
Accepted 22 SEP 2023

Abstract We describe how typical relative humidity (RH) profiles change systematically through the phases of the Madden–Julian Oscillation (MJO). We use 18 years of classified RH-profiles from the Atmospheric Infrared Sounder, clustered without prior knowledge of large-scale dynamics or occurrence-region. Occurrence probability (OP) anomalies of RH-profiles classes exhibit classical MJO patterns: Large positive OP anomalies of the RH-profile class with most moisture in the free troposphere are co-located with the largest positive precipitation anomalies. About 10 days prior to this deep convective core large OP anomalies of a RH-profile class occur consistent with lower atmospheric moistening, supporting a ubiquitous role of pre-moistening in MJO propagation. Since each RH-profile class is associated with distinct dynamics (most of which are subgrid-scale to climate models) our results can serve as process-based diagnostics to investigate parameterization shortcomings of climate models preventing them to simulate the MJO accurately.

Plain Language Summary The Madden–Julian Oscillation (MJO) is a pattern of atmospheric convection, cloudiness, and rainfall that moves eastward across the Indian and Pacific Oceans over about 30–60 days. In previous studies relative humidity (RH) profiles estimated from satellite data have been clustered into distinct classes. Here we exhibit how those RH-profile classes change systematically with the MJO. Importantly, the RH-profiles themselves do not change with the MJO, but where they occur changes: The RH-profile with largest humidity throughout the atmosphere occurs in the same places as the most convection and rainfall. East of the convective core, a profile which is moist in the lower half of the troposphere, but drier above, occurs more often; this is important in priming the atmosphere for deep convection. Results of this study can inform diagnostics for identifying why climate models struggle in representing the MJO and which moisture transition processes require refinement.

1. Introduction

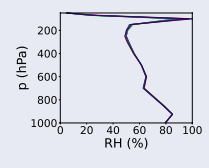
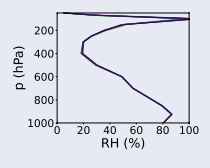
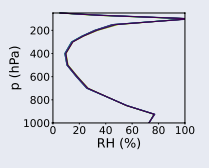
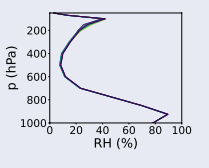
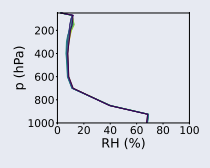
Atmospheric relative humidity (RH) profiles over Earth's oceans can be robustly clustered into 8 “primitive” classes, each of which can be associated with distinct dynamical features (Abraham & Goldblatt, 2022, 2023). The structures of these RH-classes are robust against intra- and interannual variability, hence changes in spatial water vapor distribution or atmospheric moisture transitions manifest through occurrence frequency changes of these RH-classes (e.g., Abraham & Goldblatt, 2022, 2023). Deep convection transports copious amounts of water vapor into the atmospheric column, which affects the global hydrological budget and atmosphere's radiative properties, both of which impact extreme events (e.g., Abraham & Goldblatt, 2023; Angulo-Umana & Kim, 2023; H. H. Aumann et al., 2018; Roca & Fiolleau, 2020; Stan et al., 2017; Tromeur & Rossow, 2010; Wong & Teixeira, 2016). An important tropical deep-convection pattern is associated with the Madden–Julian Oscillation (MJO; Madden & Julian, 1994). In this study we investigate how occurrence patterns of typical tropical RH-profile classes (particularly those associated with deep-convection) vary with the different phases of the MJO.

The hyperspectral Atmospheric Infrared Sounder (AIRS) on NASA's Aqua satellite allows for systematically investigating vertical structures of tropospheric water vapor content above Earth's oceans (H. Aumann et al., 2003; Kalmus et al., 2015). Abraham and Goldblatt (2022, 2023) classified AIRS RH-profiles into eight distinct and physically meaningful classes using *k*-means clustering (i.e., no predefined knowledge of occurrence region or atmospheric dynamics is applied). Each class can be associated with particular atmospheric dynamics. Five of

© 2023 His Majesty the King in Right of Canada and The Authors. Reproduced with the permission of the Minister of Environment and Climate Change Canada.

This is an open access article under the terms of the [Creative Commons Attribution-NonCommercial-NoDerivs License](https://creativecommons.org/licenses/by/4.0/), which permits use and distribution in any medium, provided the original work is properly cited, the use is non-commercial and no modifications or adaptations are made.

Table 1
Summary of the Five Distinct RH-Profile Classes That Dominate the Tropics and Subtropics (Abraham & Goldblatt, 2022)

RH-profile class	A1	A2	A3	A4	A5
	Moist		Dry		
Region	Tropics			Tropics, Subtropics	Subtropics
RH-Structure in MJO-phases					
Main characteristics of vertical RH-structure in the troposphere	almost constant RH-values (around 60%); RH-peak near tropopause	linear decrease from 80% at 925 hPa to 20% at 200 hPa; RH-peak near tropopause	“C-shape” (Roms, 2014); RH-peak near tropopause	boundary-layer top around 100% RH, dry troposphere (RH < 20%)	constant dry troposphere (RH < 15%)
Associated dynamics	convection		height variations in the water vapour lapse rate due to large-scale subsidence exceeding convective activity; RH peak could also be associated with moisture advection (Roms, 2014)		mid-latitude eddies transporting moisture along isentropes drying the subtropics (Galewsky et al., 2005)
Special features	Deep	Congestus		low-level strato-cumulus clouds	mainly clear-sky conditions

Note. The vertical structures of the RH-profiles against atmospheric pressure (p) are determined by averaging the RH-profile observations according to cluster affiliations of k-means clustering analysis (Abraham & Goldblatt, 2022) and the eight MJO phases (Wheeler & Hendon, 2004). Variability around each mean profile is low (Abraham & Goldblatt, 2022). The profiles are essentially identical for each phase, so the graphs for all eight phases are largely coincident.

these RH-classes (A1–A5) occur predominantly in the tropics and subtropics (Table 1), accounting for more than 80% of all RH-profiles retrieved in those regions (Abraham & Goldblatt, 2023). Moist profiles (A1–A2) establish in convective updraft regions, particularly in the intertropical convergence zone (ITCZ) and Indo-Pacific warm pool. Dry profiles (A3–A5) are generally associated with large-scale subsidence that suppress convective activity and allow, for instance, low-level stratocumulus clouds to form.

Mean RH-profiles of each class are robust and independent from underlying sea-surface temperatures (SST; Abraham & Goldblatt, 2022), seasons, or warming climate conditions (Abraham & Goldblatt, 2023). By contrast, the geographical conditional occurrence probabilities (OP) of each RH-class change substantially with the seasons and with warming (Abraham & Goldblatt, 2023). Increases in the OPs of convective RH-classes (A1–A2) are found to drive the OPs of other drier RH-classes, as convection is compensated by expanding dry areas with strong subsidence (Abraham & Goldblatt, 2023).

The MJO is a deep convection propagation pattern associated with negative outgoing longwave radiation (OLR) and positive precipitation anomalies moving eastward across the Indian and Pacific oceans on timescales of about 30–60 days (e.g., Madden, 1986; Madden & Julian, 1994). The overall large-scale MJO pattern can be understood as exhibiting dipole structures between suppressed and enhanced convection (Adames & Kim, 2016; Adames & Wallace, 2015). Most often, however, the MJO propagation pattern is divided into eight different phases (Ventrice et al., 2013; Wheeler & Hendon, 2004). During boreal winter (November–April) the MJO is more active and generally starts in the equatorial Indian Ocean east of Africa (phase 1) moving south-eastward across the Indo-Pacific warm-pool toward the South Pacific convergence zone (phase 8; Adames et al., 2016; Wu et al., 2006; Yu et al., 2012). During boreal summer (May–October), on the other hand, the deep convection pattern is weaker, shifted northward, and the OLR anomaly propagates north-eastward. The convection centers are preceded by moistening of the boundary layer on the eastward flank of the convective cells (Adames & Wallace, 2015; Kiladis et al., 2005).

Given that deep convection is the major MJO driver, the distribution of tropical humidity is of fundamental importance. Indeed, one major theory of MJO propagation, the moisture-mode theory, resolves the MJO as a wave in a system with moisture as the only prognostic variable (Raymond, 2001; Raymond & Fuchs, 2009; C. Zhang et al., 2020). Adames and Wallace (2015) describe the MJO moisture structure: the convective core has a westward tilt with height to the most moist regions. Descending air east and west of the moist core is drier. Up to 60° eastward of the convective core, the boundary layer is also moist, though the free troposphere remains dry, which is ascribed to moisture convergence in the boundary layer (Maloney & Hartmann, 1998). A previous satellite based climatology of MJO moisture, using older instruments, showed eastward propagating RH anomalies (Myers & Waliser, 2003).

State-of-the-art climate models struggle representing the MJO consistently (Jiang et al., 2020) or if fairly simulated the community lack understanding why those models perform well (Klingaman et al., 2015). Part of the problem is that MJO drivers, such as the deep-convection centers, radiative effects of cloud structures, or boundary layer circulations are unresolved and require subgrid-scale parameterizations (e.g., Kim & Maloney, 2017; Yang & Wang, 2019; G. J. Zhang & Song, 2009). Tuning those parameterizations to reasonably represent the MJO, particularly the deep convection schemes, usually degrades the models' mean states (Kim et al., 2011; Mapes & Neale, 2011). While resolving mesoscale circulation could allow improving the MJO propagation (M. Ahn et al., 2019; Chen & Mapes, 2018; Mapes & Neale, 2011), climate models' resolutions are still far from resolving those scales. To nonetheless improve the MJO in climate models, large-scale process-based diagnostics are required that allow identifying misrepresented processes (e.g., M.-S. Ahn et al., 2017; Jiang et al., 2020).

In summary, individual tropical RH-profiles tend to belong to a member of a relatively small set of standard moisture profiles (A1–A5), each of which has a distinct structure and physical-dynamical explanation (Abraham & Goldblatt, 2022). Systematic moisture changes manifest through OP of this set of standard profiles (Abraham & Goldblatt, 2023). In this study, we show that MJO moisture variability also manifests via systematic OP changes of the primitive RH-profiles, demonstrating how clustered RH-profiles apply not only to global scales but also to moisture transitions on smaller scales. As OPs of RH-profiles reflect the (for climate models unresolved) occurrence of atmospheric local dynamics this study provides a framework for new process-based MJO diagnostics for the climate modeling community.

2. Data and Methods

In Abraham and Goldblatt (2022) we clustered instantaneous satellite observations (about 450 million) of atmospheric RH-profiles into distinct “primitive” classes. Those RH-profiles were retrieved above Earth's oceans from AIRS on NASA's Aqua satellite between 30 August 2002 and 6 March 2021 (Kalmus et al., 2015). The AIRS Version 7 Level 2 product provides RH-values on 14 standard pressure levels between 1,000 and 50 hPa such that the vertical resolution in the middle troposphere is about 3 km, but higher and lower below and above, respectively (Maddy & Barnett, 2008). The horizontal footprint of the AIRS retrievals is approximately 45 km across. A more detailed description of the data, applied filters, and resulting uncertainties is provided in Abraham and Goldblatt (2022, 2023).

As in Abraham and Goldblatt (2022, 2023), we only use data with good quality flags ($QF \leq 1$; Susskind et al., 2003, 2006) for all of: moisture and temperature measurements on all 14 pressure levels, SST, OLR, and total cloud cover. The moisture estimates with these QFs are accurate to within 15 ppm below 300 hPa, and 6 ppm above 300 hPa (Divakarla et al., 2006; Trent et al., 2019).

In Abraham and Goldblatt (2022) we classified satellite retrieved RH-profiles using *k*-means cluster analysis. Here, we use the retrieved cluster affiliation of each RH-profile, together with time and location information, to sort RH-profiles according to MJO phases given by the real-time multivariate MJO index (Wheeler & Hendon, 2004, obtained from NOAA). Time filtering methods are not used as data are discontinuous due to applying the QFs requirements. Other MJO indices yield similar results. We restrict our analysis to the latitudinal band 35°N to 35°S, and to RH-classes A1–A5 which account for over 80% of observations in that region (Abraham & Goldblatt, 2023) (i.e., the sum of OPs illustrated do not always equal 100% because of some occurrences of classes A6–A9 in the tropics; Abraham & Goldblatt, 2022). Data availability is almost uniformly distributed in this tropical region (cf. Figure 2 in Abraham & Goldblatt, 2023).

Additionally, we investigate precipitation anomalies in the different MJO phases. The precipitation data were taken from the Tropical Rainfall Measuring Mission (TRMM) merged product 3B42 (Version 7; Huffman et al., 2007) and were available at 3 hr temporal resolution, on a 0.25° by 0.25° grid.

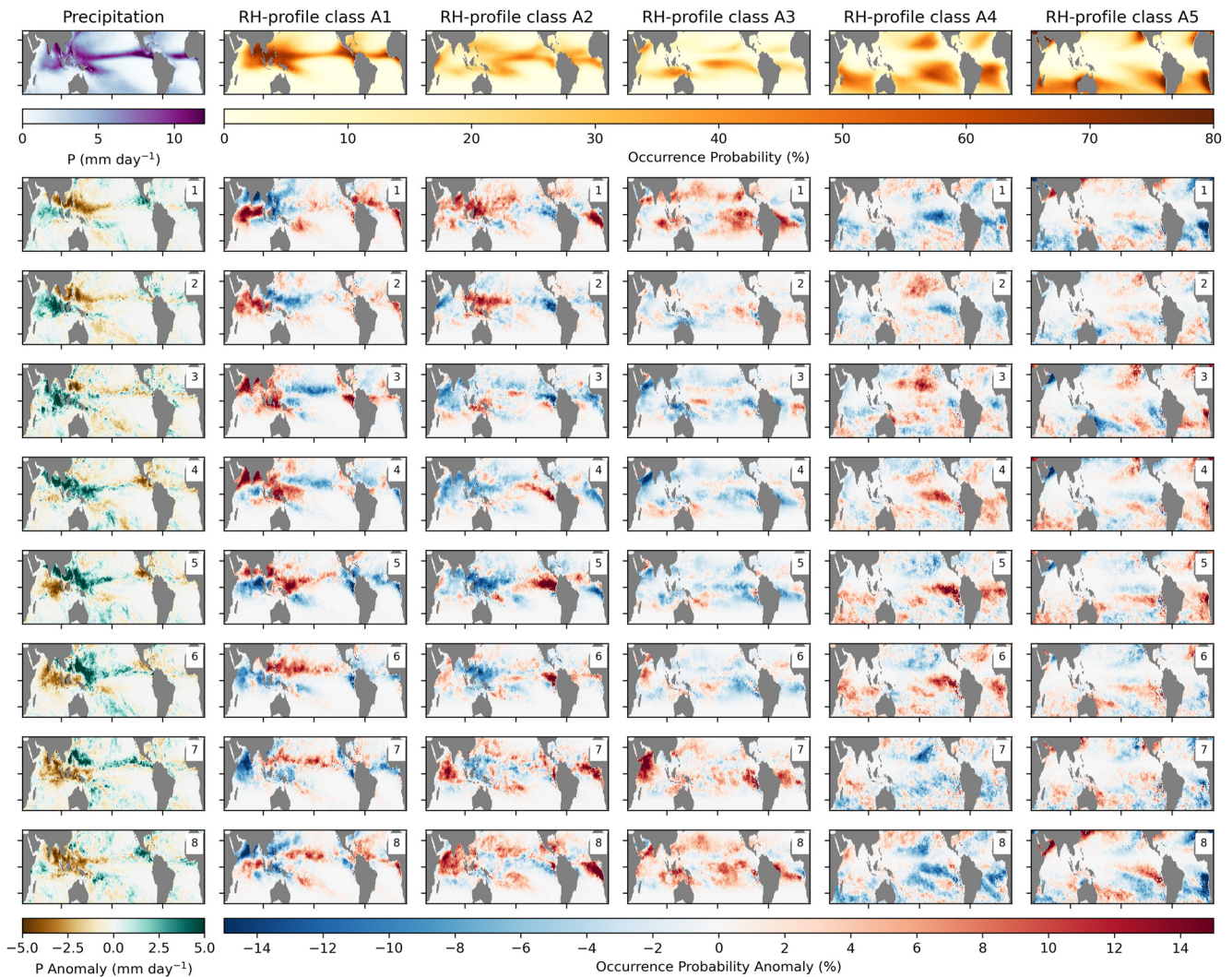


Figure 1. First Row: Climatological mean precipitation (column 1), and climatological mean occurrence probabilities of RH-profile classes A1–A5 (columns 2–6), for all-sky conditions between 35°S and 35°N between May to October (boreal summer, austral winter). Lower block: Precipitation (column 1) and occurrence probability anomalies (columns 2–6) from the climatological mean (above) of each RH-profile class in the 8 different Madden–Julian Oscillation phases.

3. Results

The composite mean structures of each RH-profile class show almost no change between the eight phases of the MJO (Table 1), with narrow RH-profile distributions around the mean (not shown, cf. Abraham & Goldblatt, 2022). This builds on previous results that the mean RH-profiles of each class are robust and independent from underlying SST (Abraham & Goldblatt, 2022), seasons, geolocation, or a warming climate (Abraham & Goldblatt, 2023); hence these standard RH-profiles occur for particular atmospheric dynamics and local dynamical changes manifest in the transition from one RH-class to another.

Since RH-structures are robust, independent of geolocation and time, atmospheric moisture transitions can be studied through the OP anomalies of each class. For the MJO we identify a remarkably clear pattern (Figures 1 and 2): Eastward propagating anomalies in the occurrence of moist profiles associated with convection, A1 and A2, are evident in summer and winter. Eastward propagating anomalies in dry profiles associated with descent are clearest in A4 in boreal summer and A3 in boreal winter. These propagating OP anomaly patterns of both moist (convection enhancing) and dry (convection suppressing) profiles build a dipole structure (cf. Adames & Kim, 2016).

In our previous work (Abraham & Goldblatt, 2022, 2023), we associated RH-profile class A1 with deep convection based on the consistently large RH throughout the troposphere (e.g., Bretherton et al., 2004), and on its

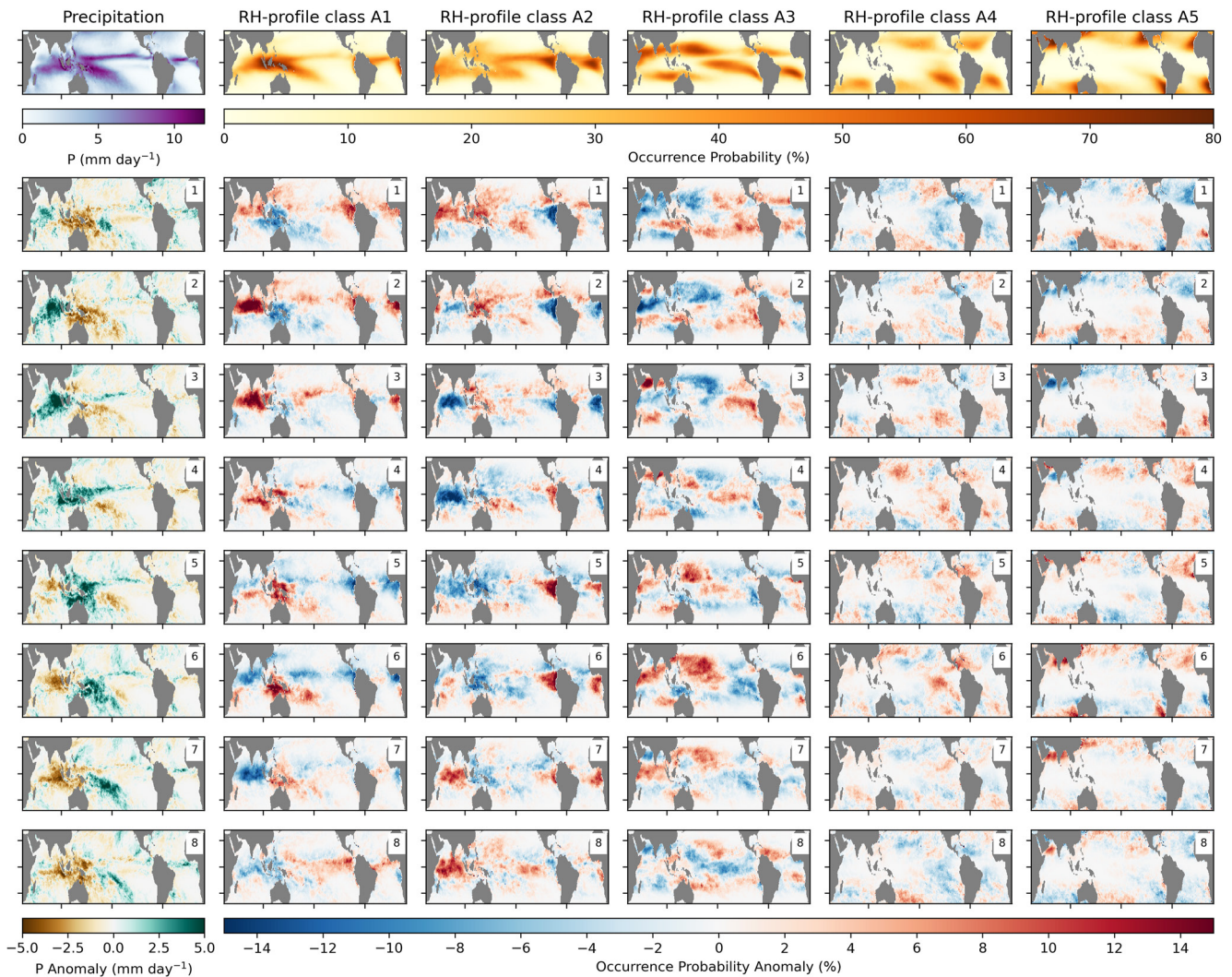


Figure 2. As Figure 1 but for the November to April (boreal winter, austral summer) season.

most frequent occurrence around the ITCZ and Indo-Pacific warm pool, regions dominated by deep convection (Raymond et al., 2003). Comparing OP anomalies of A1 with the different MJO phases provides an excellent empirical framework to substantiate this assumption. Deep convection is naturally linked to elevated precipitation. Geographical patterns of positive anomaly distributions of precipitation rates and OPs of A1 match well (Figures 1 and 2). Indeed, cross-plotting the anomaly data shows considerable positive correlation (Figure 3, first and third columns), which is strongest over the Indian Ocean and Maritime continent. Even though the linear models are not perfect (cf. p - and R^2 -values) the overall positive and negative relationships are evident.

Largest positive OP anomalies of A1 occur in convective core regions of the MJO convection centers (cf. Figures 1 and 2 with Wheeler & Hendon, 2004). These begin to form in the Indian ocean in MJO phase 1, then intensify there through MJO phase 3. Thereafter, the propagation is seasonally dependent. In boreal summer (Figure 1), positive OP anomalies of class A1 extend eastward through the Pacific in a zone north of the equator, reaching the east Pacific in MJO phase 7. We infer that this is organized along the ITCZ. In MJO phase 8, positive A1 anomalies also occur in the South Pacific Convergence Zone and in the Atlantic (although there is little anomalous precipitation there). In austral summer (Figure 2), the positive OP anomalies for class A1 extend south-eastward into the South Pacific Convergence Zone up to MJO phase 7 and remain coincident with positive precipitation anomalies, before moving east across the Pacific in MJO phase 8.

Class A2 is characterized by a moist low troposphere (Table 1), but by drier conditions in the middle and upper troposphere (typical for lower and middle atmosphere moistening with weaker precipitation from for instance

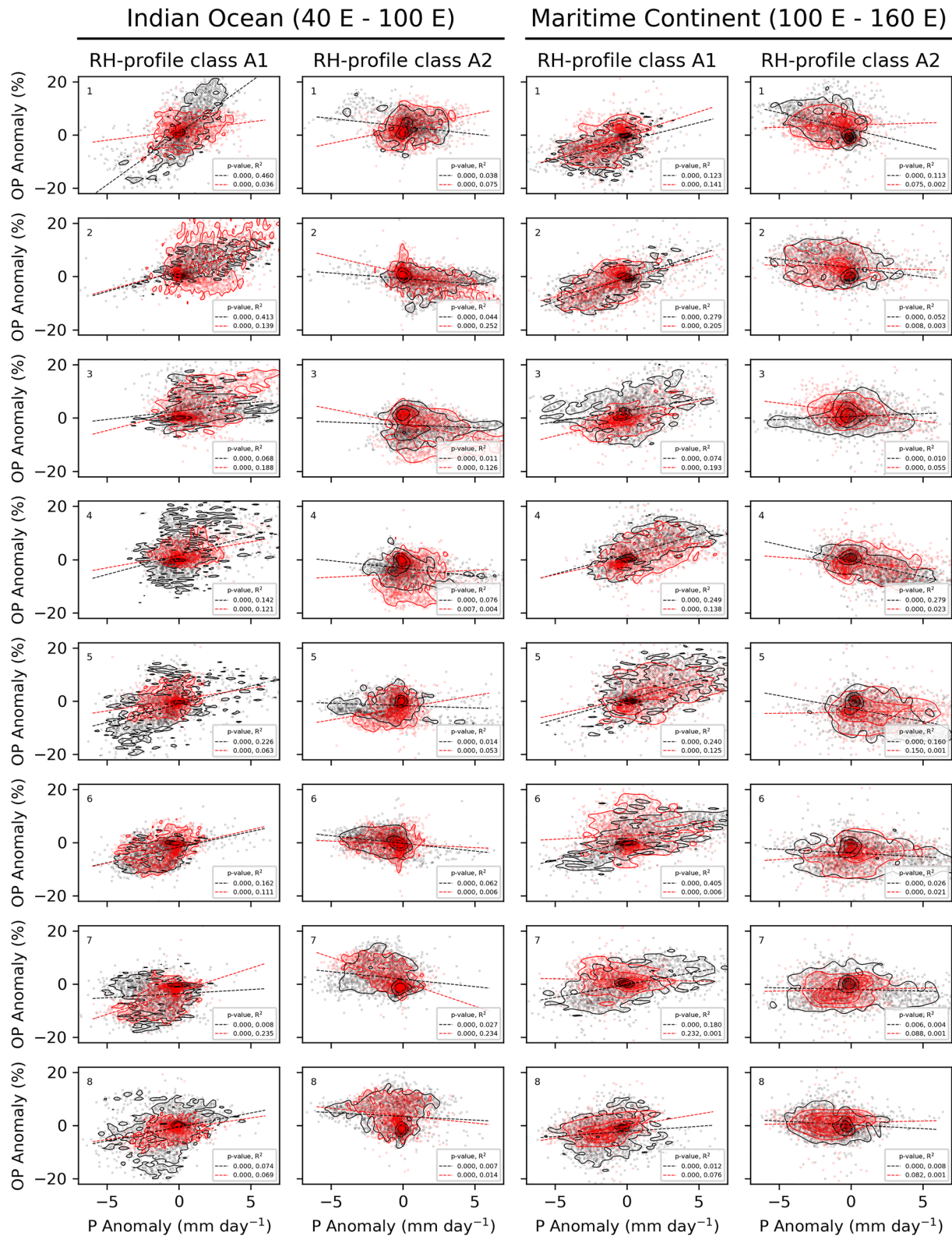


Figure 3. Scatterplot of anomalies of precipitation and OPs of RH-profile classes A1 and A2 for 20°S to 20°N in the Indian Ocean (left) and tropical Maritime continent (right) as indicated in the top panel of Figure 4 in each Madden–Julian Oscillation phase (top left number). Summer (May–October) and winter (November–April) are illustrated in black and red, respectively. Contours indicate the bivariate probability density distributions (estimated with the multivariate kernel density estimation of O’Brien et al. (2014, 2016)) and lines a linear regression model for which p -values of no linear relationship and explained variance (R^2) are displayed in the legends.

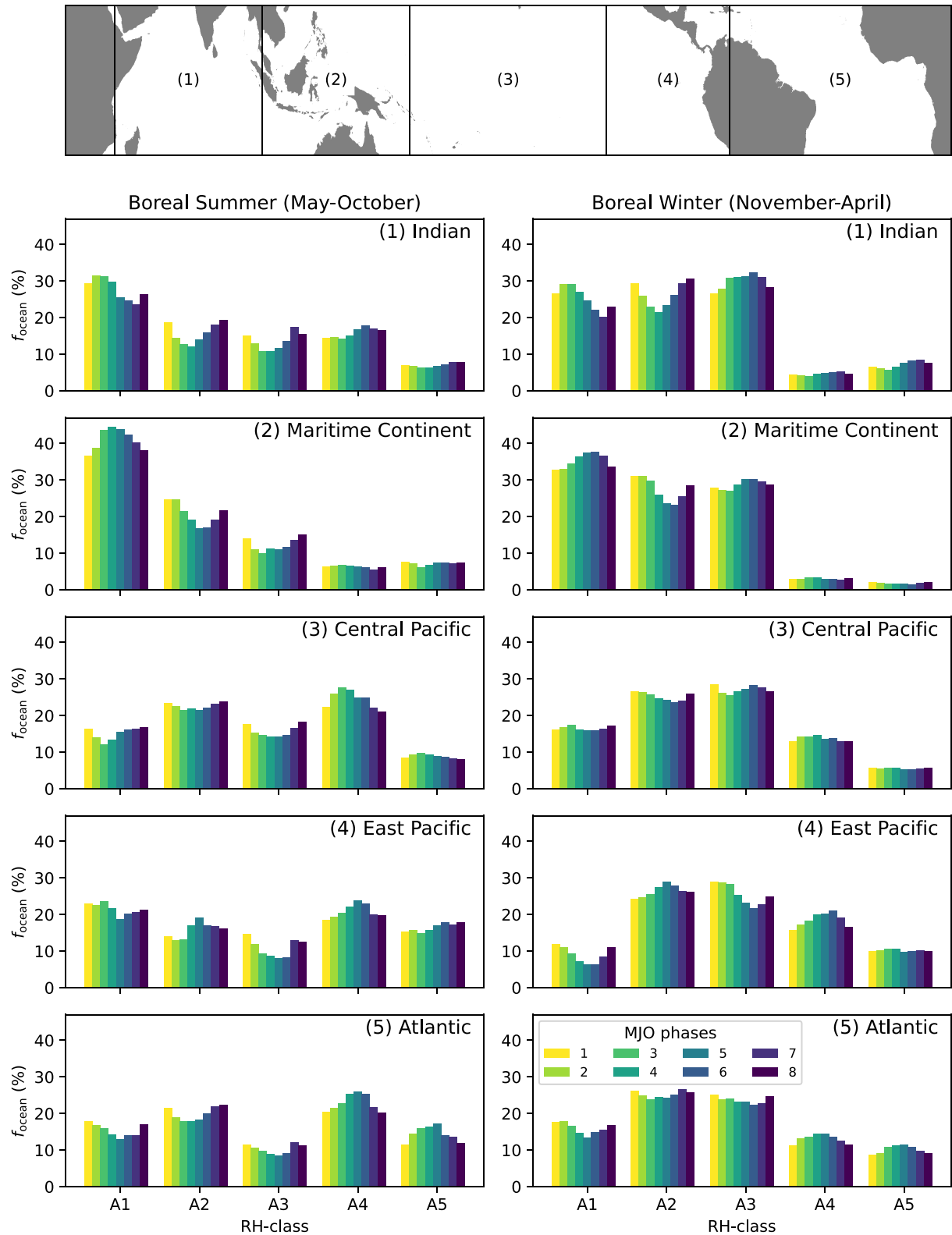


Figure 4. Ocean domain fractions between 20°N and 20°S dominated by RH-profile classes A1–A5 through the Madden–Julian Oscillation cycle in boreal summer (left) and boreal winter (right) in 5 regions (rows) as defined in map panel at the top. Ocean area fractions are calculated as in Abraham and Goldblatt (2023), and do not necessarily add up to 100% (Section 2).

congestus clouds). Consistently, OP anomalies of class A2 are anti-correlated with precipitation anomalies, as illustrated for instance over the Indian Ocean and the Maritime Continent (Figure 3). Occurrence frequency increases of A2 precede that of A1 in the eastward propagation of the MJO. During MJO phases 7–8, large positive OP anomalies of A2 are evident in the Indian Ocean, which move east to cover the warm pool region in MJO phases 1–2, before moving across the Pacific. In MJO phases 4–6, the positive OP anomalies of A2 occur over the equatorial east Pacific.

We propose that increased occurrences of RH-profile class A2 corresponds to a pre-moistening phase of the convective cycle, likely through mid-level (congestus) convection, that is responsible for MJO propagation. In other words, on average a larger presence of class A2 leads the convective core (class A1) by approximately 10 days. Particularly in MJO phases 7–2 the importance and ubiquity of this pre-moistening phase is evident. Our results are consistent with Adames and Wallace (2015) who described the evolution of the moisture structure of the MJO. They found a region of high low-troposphere humidity east of the convective core. Their analysis emphasizes the importance of moisture convergence in the boundary layer (caused by equatorial Kelvin waves excited by the convective core; Adames & Wallace, 2015). This low-level convergence supplies moisture for mid-height convection, detrainment from which moistens the free troposphere.

An interesting feature of our results is the large positive OP anomalies of class A2 in the Indian Ocean in MJO phases 7–8 (perhaps even beginning in MJO phase 6), in regions where class A2 is otherwise uncommon. These indicate the start of the convective cycle, so identifying these may predict the initiation of an MJO event.

Further insight can be gained from the calculated fraction of the ocean domain, f_{ocean} , dominated by each class (Figure 4, see Abraham and Goldblatt (2023) for method). For example, over the Indian ocean f_{ocean} (A2) is minimal in MJO phase 4 and maximal in phase 8, increasing by about 10% in both seasons. Eastward, over the Maritime Continent, the f_{ocean} (A2) cycle is shifted by about two MJO phases, with maximal extent in phases 1–2. In both regions, maximal f_{ocean} (A1) values display a 2–3 MJO phase lag (about 10 days) from f_{ocean} (A2).

Convective regions must be compensated by large-scale subsidence, which is associated with profiles A3, A4, and A5. These profiles have similar humidity structures in the marine boundary layer, but decreasing amounts of moisture above (Table 1). The OPs of A4 and A5 are correlated, whereas the OP of A3 is anti-correlated with A4 and A5 (Abraham & Goldblatt, 2023). This can be interpreted as A4 and A5 being rather similar and, depending on the dynamics, accommodation of subsidence switches between A3 and A4/A5.

In boreal summer, there is an MJO phase dependent switch between profiles A3 and A4/A5 accommodating anomalous amounts of descent (Figure 1). In MJO phases 7–1, positive OP anomalies of class A3 dominate each side of the equator throughout the Indian, Pacific and Atlantic Basins. Class A3 has the more moist upper troposphere, so would correspond to descent occurring closer to the convective core of the MJO and source of high-altitude moisture. With positive OP anomalies of class A1 on the equator (particularly during MJO phase 7), this may be explained by enhanced meridional overturning (i.e., a stronger local Hadley circulation). By contrast, during MJO phases 2–6, classes A4 and A5 exhibit the largest positive OP anomalies, and these propagate eastward across the Pacific and into the Atlantic. In particular, in phases 4–6 there are positive OP anomalies for class A4 over the equatorial Pacific and Atlantic. At this time, there is enhanced deep convection over the warm pool (see OP anomalies of A1 and precipitation anomalies), so the large-scale pattern appears to be an enhanced zonal (Walker circulation) across the Pacific, with descent further from convection, hence the drier troposphere aloft.

In austral summer, variability is dominated by class A3. In MJO phases 1 to 4, in which moist RH-profile class A1 is anomalously frequent over the Indian Ocean, positive OP anomalies in dry RH-profile class A3 are both proximal (north and south of the convection anomaly, indicating an enhanced local Hadley circulation) and distal (in the East Pacific and somewhat in the Atlantic). In MJO phases 5–7, in which moist RH-profile class A1 is anomalously frequent over the Maritime Continent, positive OP anomalies of dry RH-profile class A3 are proximal, occurring north-east of positive OP-anomalies of class A1, over the west Pacific, and west, over the Indian Ocean.

Although the MJO is primarily an Indo-Pacific phenomenon it affects the tropical convective activity in the Atlantic region (e.g., Barnston et al., 2015; Klotzbach, 2010; Yu et al., 2012). Effects on OPs of RH-classes over the Atlantic are most evident during boreal summer (Figure 1). During MJO-phases 7–2, OPs of moist RH-profile classes A1 and A2 increase along the band spanning from the equatorial Atlantic toward the Caribbean Sea. Simultaneously, OP increases of the drier class A3 are evident south of this band; to a lesser extent though in classes A4 and A5. These Atlantic moisture changes may be associated with locally enhanced African easterly

wave activity (Ventrice et al., 2011), which causes the tropical cyclone activity in the Atlantic basin toward the Caribbean Sea to increase (Barnston et al., 2015). In austral summer, the most notable Atlantic changes are switching between A1 and A2 in the equatorial east Atlantic.

4. Conclusion

Earth's RH structures vary systematically through the MJO cycle. We have examined this via a suite of five distinct RH-profiles, identified from AIRS satellite data over Earth's oceans through k-means clustering (Abraham & Goldblatt, 2022, 2023). As each RH-profile class is robust in both space and time, their spatial distributions of OP anomalies exhibit local atmospheric dynamics and systematic moisture transitions. That is, the frequency of each RH-profile class in different ocean regions changes with the MJO cycle.

The most moist RH-profile class (A1) dominates the convective core of the MJO, that is, the regions with largest vertical motions. The OP anomalies of A1 also positively correlate with positive precipitation anomalies. Second wettest RH-profile structure (A2) has a moist low-troposphere, but is drier aloft which corresponds to weaker convection. The positive OP anomalies of this RH-class lead the convective core by about 10 days. Increases in this RH-class are responsible for pre-moistening the atmosphere, and priming it for deep convection. Furthermore, RH-class A2 becomes most abundant in the Indian Ocean in MJO phases 7 and 8, which likely establishes conditions for deep convection and the initiation of a new MJO cycle. Observing large positive OP anomalies of this class might help predict the onset of an MJO event.

The progression from dry RH-profile classes A3 and A4 to A1 via A2 imparts important thermal radiative feedbacks, as moistening the mid- or upper troposphere reduces the OLR and warms the surface. Sensitivity studies by Bourdin et al. (2021) show that, at low baseline RH, moistening partially the atmosphere above 800 hPa is sufficient to allow transitions into deep convection occurrence. Thus, initiating mid-level convection primes the atmosphere and allows transitioning toward increases of class A1. Naturally, cloud radiative feedbacks play a role in the MJO propagation by anomalously heating and hence destabilizing convective areas (e.g., Arnold & Randall, 2015; Bony et al., 2015; Jiang, 2017; Kim et al., 2015); here we only discuss the pure water vapor feedbacks as we still investigate links between the distinct RH-profile classes and cloud type distributions.

The demonstrated large-scale OP behavior of typical RH-profile classes has implications for MJO modeling and MJO theory as it allows not only identifying RH anomalies but also the local atmospheric dynamics. Thus, observed ubiquitousness of the RH-profile classes and their OP changes throughout the MJO cycle can serve as a diagnostic to test the fidelity of climate models in their simulations of the MJO as many climate models still struggle in simulating the MJO accurately (Jiang et al., 2020; Le et al., 2021). Therefore, analyzing RH-profile characteristics in these models and their MJO changes would be useful to understand which atmospheric dynamics on the subgrid-scale cause misrepresentations, particularly in terms of pre-moistening the lower troposphere for eastward propagation. Similarly, different theories of the MJO such as moisture mode theory, the skeleton model, and the trio-interaction theory (C. Zhang et al., 2020) make different assumptions about the role of moisture and the processes that govern the change of moisture throughout the MJO cycle. Numerical models based on these theories can also be tested using the RH-profile metric described above, to assess the ability of the relevant theory to produce this observed behavior.

Data Availability Statement

The AIRS Version 7 Level 2 data are freely available via the Goddard Earth Sciences Data and Information Services Center (GES DISC, https://disc.gsfc.nasa.gov/datasets/AIRS2RET_7.0/summary). The GES DISC provides additional information and documentation about the AIRS L2 products and other products of interest, as well as ordering and data sub-setting tools and services. We accessed the data on 6 March 2021. The 3B42 precipitation data were provided by the NASA/Goddard Space Flight Center and PPS, which develop and compute the 3B42 data set as a contribution to the TRMM project, and archived at the NASA GES DISC. The phases of the MJO were obtained through NOAA (<https://psl.noaa.gov/mjo/mjoindex/>). Those data have been accessed on 14 May 2021. Scripts and post-processed data for plots can be found at <https://doi.org/10.5281/zenodo.8377358>.

Acknowledgments

CA was supported by the Flood Hazard Identification and Mapping Program (FHIMP) project of Environment and Climate Change Canada. CG received support from the Canadian Space Agency (Grant 16SUASOMTR) and the Natural Sciences and Engineering Research Council of Canada (NSERC; Discovery Grant RGPIN-2018-05929 and Research Tools and Equipment Grant RTI-2020-00277). AJM was partially funded by the Natural Environment Research Council through the TerraMaris project (Grant NE/R016704/1). We thank two anonymous reviewers for their suggestions and helpful comments to improve this manuscript.

References

Abraham, C., & Goldblatt, C. (2022). A satellite climatology of relative humidity profiles and outgoing thermal radiation over Earth's Oceans. *Journal of the Atmospheric Sciences*, 79(9), 2243–2265. <https://doi.org/10.1175/JAS-D-21-0270.1>

Abraham, C., & Goldblatt, C. (2023). Changes in relative humidity profiles over Earth's oceans in a warming climate: A satellite data based inference. *Journal of the Atmospheric Sciences*, 80(7), 1847–1866. <https://doi.org/10.1175/JAS-D-22-0119.1>

Adames, A. F., & Kim, D. (2016). The MJO as a dispersive, convectively coupled moisture wave: Theory and observations. *Journal of the Atmospheric Sciences*, 73(3), 913–941. <https://doi.org/10.1175/JAS-D-15-0170.1>

Adames, A. F., & Wallace, J. M. (2015). Three-dimensional structure and evolution of the moisture field in the MJO. *Journal of the Atmospheric Sciences*, 72(10), 3733–3754. <https://doi.org/10.1175/JAS-D-15-0003.1>

Adames, A. F., Wallace, J. M., & Monteiro, J. M. (2016). Seasonality of the structure and propagation characteristics of the MJO. *Journal of the Atmospheric Sciences*, 73(9), 3511–3526. <https://doi.org/10.1175/JAS-D-15-0232.1>

Ahn, M., Kim, D., Park, S., & Ham, Y. (2019). Do we need to parameterize mesoscale convective organization to mitigate the MJO-mean state trade-off? *Geophysical Research Letters*, 46(4), 2293–2301. <https://doi.org/10.1029/2018GL080314>

Ahn, M.-S., Kim, D., Sperber, K. R., Kang, I.-S., Maloney, E., Waliser, D., & Hendon, H. (2017). MJO simulation in CMIP5 climate models: MJO skill metrics and process-oriented diagnosis. *Climate Dynamics*, 49(11–12), 4023–4045. <https://doi.org/10.1007/s00382-017-3558-4>

Angulo-Umana, P., & Kim, D. (2023). Mesoscale convective clustering enhances tropical precipitation. *Science Advances*, 9(2). <https://doi.org/10.1126/sciadv.abo5317>

Arnold, N. P., & Randall, D. A. (2015). Global-scale convective aggregation: Implications for the Madden-Julian oscillation. *Journal of Advances in Modeling Earth Systems*, 7(4), 1499–1518. <https://doi.org/10.1002/2015MS000498>

Aumann, H., Chahine, M., Gautier, C., Goldberg, M., Kalnay, E., McMillin, L., et al. (2003). AIRS/AMSU/HSB on the aqua mission: Design, science objectives, data products, and processing systems. *IEEE Transactions on Geoscience and Remote Sensing*, 41(2), 253–264. <https://doi.org/10.1109/TGRS.2002.808356>

Aumann, H. H., Behrangi, A., & Wang, Y. (2018). Increased frequency of extreme tropical deep convection: AIRS observations and climate model predictions. *Geophysical Research Letters*, 45(24), 13530–13537. <https://doi.org/10.1029/2018GL079423>

Barnston, A. G., Vigaud, N., Long, L. N., Tippett, M. K., & Schemm, J.-K. E. (2015). Atlantic tropical cyclone activity in response to the MJO in NOAA's CFS model. *Monthly Weather Review*, 143(12), 4905–4927. <https://doi.org/10.1175/MWR-D-15-0127.1>

Bony, S., Stevens, B., Frierson, D. M. W., Jakob, C., Kageyama, M., Pincus, R., et al. (2015). Clouds, circulation and climate sensitivity. *Nature Geoscience*, 8(4), 261–268. <https://doi.org/10.1038/ngeo2398>

Bourdin, S., Kluft, L., & Stevens, B. (2021). Dependence of climate sensitivity on the given distribution of relative humidity. *Geophysical Research Letters*, 48(8), e2021GL092462. <https://doi.org/10.1029/2021GL092462>

Bretherton, C. S., Peters, M. E., & Back, L. E. (2004). Relationships between water vapor path and precipitation over the tropical oceans. *Journal of Climate*, 17(7), 1517–1528. [https://doi.org/10.1175/1520-0442\(2004\)017<1517:RBWVPA>2.0.CO;2](https://doi.org/10.1175/1520-0442(2004)017<1517:RBWVPA>2.0.CO;2)

Chen, B., & Mapes, B. E. (2018). Effects of a simple convective organization scheme in a two-plume GCM. *Journal of Advances in Modeling Earth Systems*, 10(3), 867–880. <https://doi.org/10.1002/2017MS001106>

Divakarla, M. G., Barnet, C. D., Goldberg, M. D., McMillin, L. M., Maddy, E., Wolf, W., et al. (2006). Validation of atmospheric infrared sounder temperature and water vapor retrievals with matched radiosonde measurements and forecasts. *Journal of Geophysical Research*, 111(D9), D09S15. <https://doi.org/10.1029/2005JD006116>

Galewsky, J., Sobel, A., & Held, I. (2005). Diagnosis of subtropical humidity dynamics using tracers of last saturation. *Journal of the Atmospheric Sciences*, 62(9), 3353–3367. <https://doi.org/10.1175/JAS3533.1>

Huffman, G. J., Bolvin, D. T., Nelkin, E. J., Wolff, D. B., Adler, R. F., Gu, G., et al. (2007). The TRMM multisatellite precipitation analysis (TMPA): Quasi-global, multiyear, combined-sensor precipitation estimates at fine scales. *Journal of Hydrometeorology*, 8(1), 38–55. <https://doi.org/10.1175/JHM560.1>

Jiang, X. (2017). Key processes for the eastward propagation of the Madden-Julian oscillation based on multimodel simulations. *Journal of Geophysical Research: Atmospheres*, 122(2), 755–770. <https://doi.org/10.1002/2016JD025955>

Jiang, X., Adames, N. F., Kim, D., Maloney, E. D., Lin, H., Kim, H., et al. (2020). Fifty years of research on the Madden-Julian oscillation: Recent progress, challenges, and perspectives. *Journal of Geophysical Research: Atmospheres*, 125(17), e2019JD030911. <https://doi.org/10.1029/2019JD030911>

Kalmus, P., Sun, W., & Teixeira, J. (2015). The Pacific subtropical cloud transition: A MAGIC assessment of AIRS and ECMWF thermodynamic structure. *IEEE Geoscience and Remote Sensing Letters*, 12(7), 1586–1590. <https://doi.org/10.1109/LGRS.2015.2413771>

Kiladis, G. N., Straub, K. H., & Haertel, P. T. (2005). Zonal and vertical structure of the Madden-Julian oscillation. *Journal of the Atmospheric Sciences*, 62(8), 2790–2809. <https://doi.org/10.1175/JAS3520.1>

Kim, D., Ahn, M.-S., Kang, I.-S., & Del Genio, A. D. (2015). Role of longwave cloud–radiation feedback in the simulation of the Madden-Julian oscillation. *Journal of Climate*, 28(17), 6979–6994. <https://doi.org/10.1175/JCLI-D-14-00767.1>

Kim, D., & Maloney, E. D. (2017). Simulation of the Madden-Julian oscillation using general circulation models. *World Scientific Series on Asia-Pacific Weather and Climate*, 9, 119–130. https://doi.org/10.1142/9789813200913_0009

Kim, D., Sobel, A. H., Maloney, E. D., Frierson, D. M. W., & Kang, I.-S. (2011). A systematic relationship between intraseasonal variability and mean state bias in AGCM simulations. *Journal of Climate*, 24(21), 5506–5520. <https://doi.org/10.1175/2011JCLI4177.1>

Klingaman, N. P., Woolnough, S. J., Jiang, X., Waliser, D., Xavier, P. K., Petch, J., et al. (2015). Vertical structure and physical processes of the Madden-Julian oscillation: Linking hindcast fidelity to simulated diabatic heating and moistening. *Journal of Geophysical Research: Atmospheres*, 120(10), 4690–4717. <https://doi.org/10.1002/2014JD022374>

Klotzbach, P. J. (2010). On the Madden-Julian oscillation–Atlantic Hurricane relationship. *Journal of Climate*, 23(2), 282–293. <https://doi.org/10.1175/2009JCLI2978.1>

Le, P. V. V., Guilloteau, C., Mamalakis, A., & Fofoula-Georgiou, E. (2021). Underestimated MJO variability in CMIP6 models. *Geophysical Research Letters*, 48(12), e2020GL092244. <https://doi.org/10.1029/2020GL092244>

Madden, R. A. (1986). Seasonal variations of the 40–50 day oscillation in the tropics. *Journal of the Atmospheric Sciences*, 43(24), 3138–3158. [https://doi.org/10.1175/1520-0469\(1986\)043<3138:SVOTDO>2.0.CO;2](https://doi.org/10.1175/1520-0469(1986)043<3138:SVOTDO>2.0.CO;2)

Madden, R. A., & Julian, P. R. (1994). Observations of the 40–50-day tropical oscillation—A review. *Monthly Weather Review*, 122(5), 814–837. [https://doi.org/10.1175/1520-0493\(1994\)122<0814:OOTDIO>2.0.CO;2](https://doi.org/10.1175/1520-0493(1994)122<0814:OOTDIO>2.0.CO;2)

Maddy, E. S., & Barnet, C. D. (2008). Vertical resolution estimates in version 5 of airs operational retrievals. *IEEE Transactions on Geoscience and Remote Sensing*, 46(8), 2375–2384. <https://doi.org/10.1109/TGRS.2008.917498>

- Maloney, E. D., & Hartmann, D. L. (1998). Frictional moisture convergence in a composite life cycle of the Madden-Julian oscillation. *Journal of Climate*, *11*(9), 2387–2403. [https://doi.org/10.1175/1520-0442\(1998\)011<2387:FMCIAC>2.0.CO;2](https://doi.org/10.1175/1520-0442(1998)011<2387:FMCIAC>2.0.CO;2)
- Mapes, B., & Neale, R. (2011). Parameterizing convective organization to escape the entrainment dilemma. *Journal of Advances in Modeling Earth Systems*, *3*(2). <https://doi.org/10.1029/2011MS000042>
- Myers, D. S., & Waliser, D. E. (2003). Three-dimensional water vapor and cloud variations associated with the Madden-Julian oscillation during Northern Hemisphere winter. *Journal of Climate*, *16*(6), 929–950. [https://doi.org/10.1175/1520-0442\(2003\)016<0929:TDWVAC>2.0.CO;2](https://doi.org/10.1175/1520-0442(2003)016<0929:TDWVAC>2.0.CO;2)
- O'Brien, T. A., Collins, W. D., Rauscher, S. A., & Ringler, T. D. (2014). Reducing the computational cost of the ECF using a nuFFT: A fast and objective probability density estimation method. *Computational Statistics & Data Analysis*, *79*, 222–234. <https://doi.org/10.1016/j.csda.2014.06.002>
- O'Brien, T. A., Kashinath, K., Cavanaugh, N. R., Collins, W. D., & O'Brien, J. P. (2016). A fast and objective multidimensional Kernel density estimation method: FastKDE. *Computational Statistics & Data Analysis*, *101*, 148–160. <https://doi.org/10.1016/j.csda.2016.02.014>
- Raymond, D. J. (2001). A new model of the Madden-Julian oscillation. *Journal of the Atmospheric Sciences*, *58*(18), 2807–2819. [https://doi.org/10.1175/1520-0469\(2001\)058<2807:ANMOTM>2.0.CO;2](https://doi.org/10.1175/1520-0469(2001)058<2807:ANMOTM>2.0.CO;2)
- Raymond, D. J., & Fuchs, Z. (2009). Moisture modes and the Madden-Julian oscillation. *Journal of Climate*, *22*(11), 3031–3046. <https://doi.org/10.1175/2008JCLI2739.1>
- Raymond, D. J., Raga, G. B., Bretherton, C. S., Molinari, J., Lopez-Carrillo, C., & Fuchs, Z. (2003). Convective forcing in the intertropical convergence zone of the Eastern Pacific. *Journal of the Atmospheric Sciences*, *60*(17), 2064–2082. [https://doi.org/10.1175/1520-0469\(2003\)060<2064:CFITIC>2.0.CO;2](https://doi.org/10.1175/1520-0469(2003)060<2064:CFITIC>2.0.CO;2)
- Roca, R., & Fiolleau, T. (2020). Extreme precipitation in the tropics is closely associated with long-lived convective systems. *Communications Earth & Environment*, *1*(1), 18. <https://doi.org/10.1038/s43247-020-00015-4>
- Roms, D. M. (2014). An analytical model for tropical relative humidity. *Journal of Climate*, *27*(19), 7432–7449. <https://doi.org/10.1175/JCLI-D-14-00255.1>
- Stan, C., Straus, D. M., Frederiksen, J. S., Lin, H., Maloney, E. D., & Schumacher, C. (2017). Review of tropical-extratropical teleconnections on intraseasonal time scales. *Reviews of Geophysics*, *55*(4), 902–937. <https://doi.org/10.1002/2016RG000538>
- Susskind, J., Barnet, C., & Blaisdell, J. (2003). Retrieval of atmospheric and surface parameters from AIRS/AMSU/HSB data in the presence of clouds. *IEEE Transactions on Geoscience and Remote Sensing*, *41*(2), 390–409. <https://doi.org/10.1109/TGRS.2002.808236>
- Susskind, J., Barnet, C., Blaisdell, J., Iredell, L., Keita, F., Kouvaris, L., et al. (2006). Accuracy of geophysical parameters derived from atmospheric infrared sounder/advanced microwave sounding unit as a function of fractional cloud cover. *Journal of Geophysical Research*, *111*(D9), D09S17. <https://doi.org/10.1029/2005JD006272>
- Trent, T., Schröder, M., & Remedios, J. (2019). GEWEX water vapor assessment: Validation of AIRS tropospheric humidity profiles with characterized radiosonde soundings. *Journal of Geophysical Research: Atmospheres*, *124*(2), 886–906. <https://doi.org/10.1029/2018JD028930>
- Tromeur, E., & Rossow, W. B. (2010). Interaction of tropical deep convection with the large-scale circulation in the MJO. *Journal of Climate*, *23*(7), 1837–1853. <https://doi.org/10.1175/2009JCLI3240.1>
- Ventrice, M. J., Thorncroft, C. D., & Roundy, P. E. (2011). The Madden-Julian oscillation's influence on African easterly waves and downstream tropical cyclogenesis. *Monthly Weather Review*, *139*(9), 2704–2722. <https://doi.org/10.1175/MWR-D-10-05028.1>
- Ventrice, M. J., Wheeler, M. C., Hendon, H. H., Schreck, C. J., Thorncroft, C. D., & Kiladis, G. N. (2013). A modified multivariate Madden-Julian oscillation index using velocity potential. *Monthly Weather Review*, *141*(12), 4197–4210. <https://doi.org/10.1175/MWR-D-12-00327.1>
- Wheeler, M. C., & Hendon, H. H. (2004). An all-season real-time multivariate MJO Index: Development of an index for monitoring and prediction. *Monthly Weather Review*, *132*(8), 1917–1932. [https://doi.org/10.1175/1520-0493\(2004\)132<1917:AARMMI>2.0.CO;2](https://doi.org/10.1175/1520-0493(2004)132<1917:AARMMI>2.0.CO;2)
- Wong, S., & Teixeira, J. (2016). Extreme convection and tropical climate variability: Scaling of cold brightness temperatures to sea surface temperature. *Journal of Climate*, *29*(10), 3893–3905. <https://doi.org/10.1175/JCLI-D-15-01214.1>
- Wu, M.-L. C., Schubert, S. D., Suarez, M. J., Pegion, P. J., & Waliser, D. E. (2006). Seasonality and meridional propagation of the MJO. *Journal of Climate*, *19*(10), 1901–1921. <https://doi.org/10.1175/JCLI3680.1>
- Yang, Y.-M., & Wang, B. (2019). Improving MJO simulation by enhancing the interaction between boundary layer convergence and lower tropospheric heating. *Climate Dynamics*, *52*(7–8), 4671–4693. <https://doi.org/10.1007/s00382-018-4407-9>
- Yu, W., Han, W., & Gochis, D. (2012). Influence of the Madden-Julian oscillation and intraseasonal waves on surface wind and convection of the tropical Atlantic Ocean. *Journal of Climate*, *25*(23), 8057–8074. <https://doi.org/10.1175/JCLI-D-11-00528.1>
- Zhang, C., Adames, A. F., Khouider, B., Wang, B., & Yang, D. (2020). Four theories of the Madden-Julian oscillation. *Reviews of Geophysics*, *58*(3). <https://doi.org/10.1029/2019RG000685>
- Zhang, G. J., & Song, X. (2009). Interaction of deep and shallow convection is key to Madden-Julian Oscillation simulation. *Geophysical Research Letters*, *36*(9), L09708. <https://doi.org/10.1029/2009GL037340>